

Synthesis, structural characterization, photoluminescence and thermal properties of $[(\text{Ph}_3\text{P})_2\text{Cu}(\mu\text{-SeC}\{\text{O}\}\text{R})_2\text{Cu}(\text{PPh}_3)]^\dagger$

Zheng Lu,^a Wei Huang^b and Jagadese J. Vittal^a

^a Department of Chemistry, National University of Singapore, 3 Science Drive, Singapore 117543

^b Institute of Materials Science and Engineering, 3 Science Link, Singapore 117602

Received (in London, UK) 9th April 2002, Accepted 31st May 2002

First published as an Advance Article on the web 12th July 2002

A number of neutral unsymmetrical dimers $[(\text{Ph}_3\text{P})_2\text{Cu}(\mu\text{-SeC}\{\text{O}\}\text{R})_2\text{Cu}(\text{PPh}_3)]$ ($\text{R} = \text{C}_6\text{H}_5$ (**1**), $\text{C}_6\text{H}_4\text{-Me-4}$ (**2**), $\text{C}_6\text{H}_4\text{-OMe-4}$ (**3**), $\text{C}_6\text{H}_4\text{-Cl-4}$ (**4**), $\text{C}_6\text{H}_4\text{-F-4}$ (**5**) and CH_3 (**6**)) were synthesized in moderate yield, and characterized by analytical and spectroscopic techniques including ^{31}P NMR. Variable temperature ^{31}P NMR experiments appear to indicate that the molecular structure is retained in solution. X-Ray structure determination of **2** and **6** confirmed the molecular geometry of the unsymmetrical dimer. In **2** the two 4-MeO- $\text{C}_6\text{H}_4\text{C=O}$ groups have *anti* stereochemistry with respect to the Cu_2Se_2 ring while MeC=O groups have *syn* configuration in **6**. A weak $\text{C-H}\cdots\text{O=C}$ intramolecular hydrogen bond present between the two selenoacetato ligands appears to dictate the *syn* geometry in **6**. This hydrogen bonding is also responsible for the non-planarity of the Cu_2Se_2 ring. These compounds are photoemissive in CH_2Cl_2 solution. Thermogravimetry and pyrolysis experiments in nitrogen atmosphere show that **1–6** are good single source precursors to copper selenide bulk materials. Preliminary experiments show that these compounds are good single source molecular precursors for cubic phase Cu_{2-x}Se nanoparticles with an average size of 75 ± 15 nm.

Introduction

The chalcogenate chemistry of the main group elements has continued to attract considerable attention in recent years due to the fact that the main group chalcogenolates can be potentially used as single-source precursors for the low-temperature synthesis of semiconductor bulk materials. Further the bonding between metals and the heavier chalcogens is relatively unexplored as compared to the corresponding sulfur analogues. For instance, a number of thiocarboxylate metal complexes have been synthesized and well characterized.^{1–6} Some of them have been shown to be good single source precursors for sulfide materials.^{1,2} For copper thiocarboxylate, Speier *et al.* first reported a triphenylphosphine adduct of a Cu(I) thiocarboxylate complex with an unsymmetrical dimeric structure⁴ in 1991. Recently, a number of triphenylphosphine adducts of Cu(I) thiocarboxylate complexes have been successfully isolated in our lab.³ In contrast, to the best of our knowledge, no selenocarboxylate complex of group 11 metals is known and only a few transition metal selenocarboxylate complexes have been reported.^{7–10}

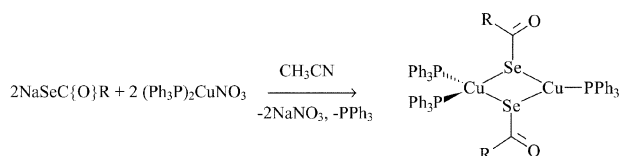
Copper selenide has been widely used in solar cells,¹¹ as an optical filter,¹² and superionic materials.¹³ In the last few years many synthetic methods for copper selenide have been reported. For example, Qian and his coworkers have successfully obtained nanocrystalline Cu_{2-x}Se at room temperature by γ -irradiation of copper acetate and sodium selenosulfate.¹⁴ On the other hand, the reaction of Cu and Se in *n*-butylamine gave crystalline Cu_{2-x}Se .¹⁵ Single source routes to copper selenide, on the other hand, are rare. $\text{Cu}(\text{SePy})_4$ and $\text{Cu}(\text{SePy}^*)_4$ (where $\text{SePy} = 2\text{-Se-NC}_3\text{H}_7$ and $\text{SePy}^* = 3\text{-Me}_3\text{Si-2-Se-NC}_3\text{H}_7$) were found to decompose to a mixture of CuSe and CuSe_2 .¹⁶ O'Brien *et al.* have used $\text{Cu}(\text{Se}_2\text{CNEt}_2)_2$ for Cu_{2-x}Se Se nanoparticles.¹⁷ However, the synthetic procedure of this precursor involves highly toxic CSe_2 .

Recent investigation in our lab on the $\text{PPh}_3\text{:Cu(I):RC}\{\text{O}\}\text{S}^-$ system led to the isolation of structurally diversified compounds ranging from mononuclear, dinuclear to two different tetranuclear aggregates.³ Each neutral derivative was found to thermally decompose to a particular phase of Cu_2S or Cu_{2-x}S for which several crystalline phases are well known.¹⁸ This study naturally gives rise to the following questions: Is there a parallel chemistry for selenocarboxylato ligand? Will $\text{RC}\{\text{O}\}\text{Se}^-$ ligand chemistry exhibit similar structural diversity? Can these be used as single-source precursors for $\text{Cu}_2\text{Se}/\text{Cu}_{2-x}\text{Se}$ materials? We wish to address these questions and hence have undertaken a project on stable neutral copper selenocarboxylate compounds containing triphenylphosphine. The compounds synthesized have been characterized by standard analytical and spectroscopic techniques and the solid state structures of representative compounds have been determined by X-ray crystallography. We have also investigated the photoluminescence properties of these compounds. Thermoanalytical techniques, especially TG, have been employed to investigate their thermal properties and the formation of the expected copper selenide was determined by the residual weight observed. Further it was thought worthwhile to study the influence of the nature of the substituents at the *para* position of the phenyl ring on the thermal stability, if any, and the final products of decomposition. We have, therefore, prepared a few phenyl derivatives of selenocarboxylato ligands and their complexes with Cu(I). The final products of thermal decomposition obtained in pyrolysis experiments were characterized by X-ray powder diffraction methods and Scanning Electron Microscopy. Preparation of nanoparticle Cu_{2-x}Se is also explored. The results of our findings are discussed in this paper.

† Electronic supplementary information (ESI) available: XRPD patterns and SEM images of the residues from pyrolysis of **1–6**. See <http://www.rsc.org/suppdata/nj/b2/b203466b/>

Results and discussion

Sodium selenocarboxylates were prepared by the literature method from Na₂Se and acid chlorides, and were allowed to react with [(Ph₃P)₂Cu(NO₃)] to get the neutral unsymmetrical dimer, [(Ph₃P)₂Cu(μ-SeC{O}R)₂Cu(PPh₃)], as shown below. A number of derivatives of selenocarboxylates has been prepared in low to moderate yield (30–63%). Interestingly, this is the only product isolated by varying the Ph₃P:Cu(I):RC{O}Se⁻ ligand ratio and experimental conditions.



R = C₆H₅ (1), CH₃-*p*-C₆H₄ (2), CH₃O-*p*-C₆H₄ (3), Cl-*p*-C₆H₄ (4), F-*p*-C₆H₄ (5), CH₃ (6) (1)

Several attempts to get a compound with a 1:1 ratio of Cu(I):PPh₃ using [(Ph₃P)CuCl] in the same way only gave the unsymmetrical dimer compound. It is rather surprising that the selenocarboxylate ligands behave differently from the thiocarboxylate ligands toward Cu(I) in the presence of PPh₃. Further, the substitution (whether it is alkyl or aryl) has no effect on the end product formation. The color of the compounds varies from dark brown to pale yellow. The compounds are soluble in CH₂Cl₂, CHCl₃ and THF, but insoluble in MeCN and MeOH. These aromatic selenocarboxylate complexes are thermally stable in air at room temperature for more than a month without any observable decomposition except 6, which can be stored for a long time in the refrigerator below 0 °C.

The carbonyl stretching frequencies of complexes 1–6 which appear in the region 1617–1657 cm⁻¹ have higher wavenumbers than those of the corresponding alkali-metal salts (1500–1560 cm⁻¹)^{18,19} but are lower than the corresponding Se-alkyl and aryl esters (1660–1720 cm⁻¹).^{20,21} Further, they occur at higher frequencies than in the corresponding thiocarboxylates (1553 cm⁻¹).⁴ However, these fall in the same region, 1610–1645 cm⁻¹, observed in [M(SeC{O}R)₂(PR'₃)₂] (M = Ni, Pt, Pd; R = Me, Ph, 2-MeC₆H₄, 4-MeC₆H₄; R' = Et, Ph).⁹

VT ³¹P NMR studies in solution

Variable temperature ³¹P NMR spectra of 1 are displayed in Fig. 1. Compound 1 gives a singlet at -0.66 ppm (Δ*v*_{1/2} = 83 Hz), at room temperature, which is as a result of rapid exchange of PPh₃ ligands in CD₂Cl₂ solution. When the solution is cooled to 273 K the signal is very broad indicating that

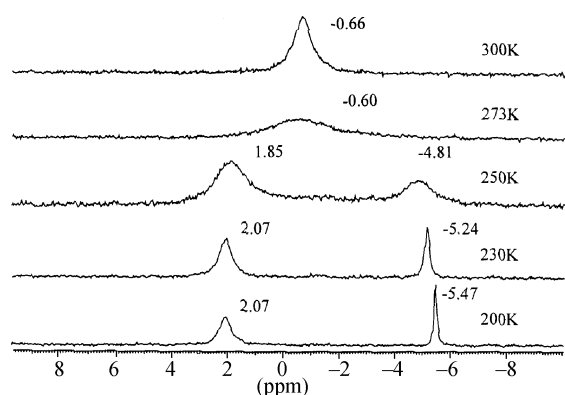


Fig. 1 Variable temperature ³¹P NMR of 1 in CD₂Cl₂ solution.

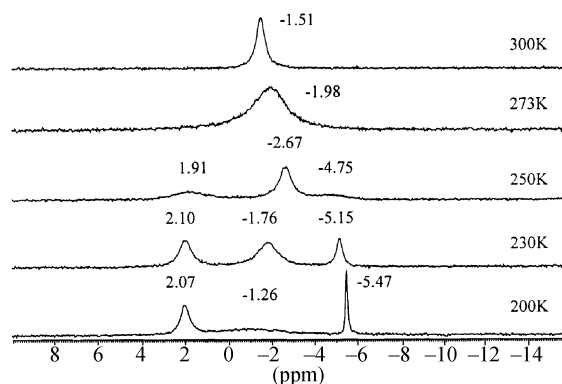


Fig. 2 VT ³¹P NMR of 1 and PPh₃ in 1:1 ratio in CD₂Cl₂ solution.

it is closer to the coalescent point, which occurs around 270 K (not shown). Below the coalescence temperature is the slow exchange region and the two ³¹P NMR signals start appearing. On cooling these signals sharpen at 2.07 (Δ*v*_{1/2} = 61 Hz) and -5.47 (Δ*v*_{1/2} = 15 Hz) at 200 K and precipitation occurs below 200 K. The integration of the intensities of these two peaks gives a ratio of 2:1 and appears to support the number of phosphorus atoms attached to Cu(1) and Cu(2) respectively in 1.

We were unable to isolate the monomer [(Ph₃P)₂Cu(SeCOR)] or symmetrical dimer [(Ph₃P)₂Cu(SeCOR)₂Cu(PPh₃)₂] and hence we have investigated whether these compounds exist in solution by ³¹P NMR studies. The VT ³¹P NMR spectra of a 1:PPh₃ mixture shown in Fig. 2 contain a signal at -1.51 (Δ*v*_{1/2} = 57 Hz) at 300 K. On cooling to 273 K, the signal broadens and moves slightly to higher field. At 250 K two more signals at δ 1.91 and -4.75 appear. The peak at -2.67 ppm starts broadening and is shifted to -1.76 at 230 K and almost disappears at 200 K while the other two signals are positioned at 2.07 and -5.47 respectively.

By comparing the chemical shifts, the shape and intensities of the signals at 2.07 and -5.47 ppm, it is tempting to conclude that these are due to the presence of [(Ph₃P)₂Cu(SeCOPh)₂Cu(PPh₃)], 1, as in Fig. 1 and the signal between these two chemical shifts may be due to exchange between 1 and PPh₃ at higher temperature, which is still present at 200 K. However there is no signal observed in the ³¹P NMR spectra due to free PPh₃ to support this assignment. The signal at -5.47 ppm is relatively sharp as compared to the other signals suggesting that it may be due to free PPh₃. The peak at δ = 2.07 in Fig. 1 may then be assigned to the symmetrical dimer with one PPh₃ attached to each Cu implying that dissociation occurred in solution. The relative broadening of this peak may be due to the quadrupoles of the Cu isotopes. The signal at -1.76 ppm at 230 K (in Fig. 2) could then be from the PPh₃ attached to tetrahedral Cu(I) of the unsymmetrical dimer. The reason that it broadens at 200 K is because the exchange of PPh₃ between the inequivalent ends is slowing. However, there is no evidence observed for the presence of excess PPh₃ in CH₂Cl₂ solution containing 1 and PPh₃ in the ESI-MS experiments and hence this alternative assignment may be ruled out.

The structures of representative compounds 2 and 6 have been determined by single crystal X-ray diffraction methods and are described in detail below.

Structure of 2

A perspective view of the molecule is illustrated in Fig. 3. Selected bond distance and angles are given in Table 1. The dimer contains one three- and one four-coordinate Cu(I) atom which are bridged by selenium atoms of two *p*-methylbenzenecarboxylate ligands. The geometry of Cu(1) is distorted tetrahedral with two PPh₃ ligands attached, while Cu(2) has a

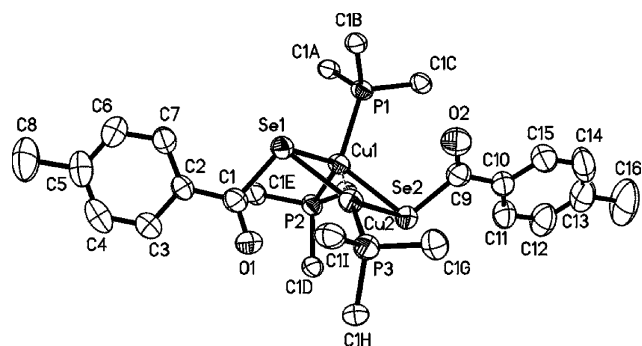


Fig. 3 Thermal ellipsoid (50% probability) diagram of **2** in which only the *ipso* C atoms of the phenyl rings are shown. The hydrogen atoms are omitted for clarity.

trigonal planar geometry with a PPh₃ ligand bonded to it. The angles around Cu(2) sum up to 359.7(1)° thus confirming the planar geometry. The tetrahedral angle around Cu(1) varies from 98.42(4) to 118.24(4)°. The structure of **2** is isomorphous and isostructural to the sulfur analogue.⁴

The Cu(i)–P distances, 2.290(1) and 2.284(1) Å, are longer than the Cu(2)–P(2) distance, 2.241(2) Å. The observed difference is due to the tetrahedral and trigonal planar geometries around the Cu(1) and Cu(2) centers respectively. The same is true for Cu–Se distances also. Cu–Se distances of 2.5390(8) Å and 2.5088(8) Å at the tetrahedral Cu(1) atom are also longer than the Cu(2)–Se(1) and Cu(2)–Se(2) distances (2.4108(8) and 2.4277(8) Å respectively) at the trigonal Cu(2) center. The disparity in Cu–Se distances due to tetrahedral and trigonal geometries is also found in [Ph₃Cu(μ-SePh)₂-Cu(PPh₃)₂]-CH₃CN (tetrahedral 2.617(1) and 2.482(1) Å and trigonal 2.406(1) and 2.416(1) Å).²² The average Cu(i)–Se distance found in [(Ph₃P)₂CuIn(SeEt)₄] is 2.526 Å.²³ The Cu–Se distances around both the tetrahedral and trigonal copper atoms are longer than 2.37 Å in (Ph₄P)₂[Cu₄(Se₄)_{2.4}(Se₅)_{0.6}] and 2.325 Å in [(Ph₄P)₄(Cu₂Se₁₄)].^{24,25}

The four-membered Cu₂Se₂ ring is strictly planar ($\Sigma \angle \text{Cu}_2\text{Se}_2 = 359.99^\circ$, with the mean deviation of the plane 0.0032 Å) and approximately assumes the shape of a parallelogram. The Cu₂Se₂P₃ core has approximate C₂ symmetry with the C₂-axis passing through Cu(1), Cu(2) and P(3). The Cu(1)–Se(1)–Cu(2) and Cu(1)–Se(2)–Cu(2) angles, 64.16(2) and 63.39(2)° respectively, are comparable to other similar angles (range, 65.91(3)–67.95(3)°) observed in the literature.²² The Se–Cu–Se angles (111.86(3) and 119.58(3)°) are obtuse and this naturally brings the two Cu atoms closer together. The Cu(1)···Cu(2) distance, 2.6311(8) Å, observed here is similar to 2.62 Å in [(Ph₃P)Cu(μ-SC{O}Ph)₂Cu(PPh₃)₂][†] and

Table 1 Selected bond lengths (Å) and angles (°) for **2**

Bond Lengths			
Cu(1)–P(1)	2.290(1)	Cu(2)–Se(2)	2.4277(8)
Cu(1)–P(2)	2.284(1)	Se(1)–C(1)	1.925(5)
Cu(2)–P(3)	2.241(2)	Se(2)–C(9)	1.932(5)
Cu(1)–Se(1)	2.5390(8)	O(1)–C(1)	1.211(6)
Cu(1)–Se(2)	2.5088(8)	O(2)–C(9)	1.203(6)
Cu(2)–Se(1)	2.4108(8)	Cu(1)–Cu(2)	2.6311(8)
Bond Angles			
P(2)–Cu(1)–P(1)	116.25(5)	Se(1)–Cu(2)–Se(2)	119.58(3)
P(2)–Cu(1)–Se(2)	98.42(4)	C(1)–Se(1)–Cu(2)	93.2(2)
P(1)–Cu(1)–Se(2)	113.14(4)	C(1)–Se(1)–Cu(1)	109.2(2)
P(2)–Cu(1)–Se(1)	118.24(4)	Cu(2)–Se(1)–Cu(1)	64.16(2)
P(1)–Cu(1)–Se(1)	99.64(4)	C(9)–Se(2)–Cu(2)	100.8(2)
Se(2)–Cu(1)–Se(1)	111.86(3)	C(9)–Se(2)–Cu(1)	104.2(2)
P(3)–Cu(2)–Se(1)	127.04(5)	Cu(2)–Se(2)–Cu(1)	64.39(2)
P(3)–Cu(2)–Se(2)	113.06(5)		

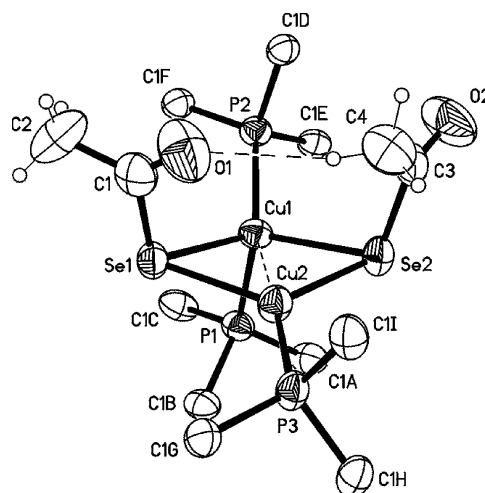


Fig. 4 The molecular structure of **6** showing the C–H···O interaction. Only the *ipso* C atoms of the phenyl rings are shown for clarity.

shorter than the sum of the van der Waals radii of Cu(i), 2.8 Å.²⁶ Further, the two *p*-methylbenzenecarboxylato ligands adopt *anti* stereochemistry in the Cu₂Se₂ ring. The C–C(=O)Se plane and the benzene ring are twisted by 3.8(4) and 9.0(3)° in the two ligands which are very normal.^{3,5,6} The structure of **2** in general is quite similar to the sulfur analogue [(Ph₃P)Cu(μ-SC{O}Ph)₂Cu(PPh₃)₂][†] reported by Speier *et al.*

Structure of 6

A perspective view of **6** is shown in Fig. 4. Selected bond distance and angles are given in Table 2. The dimer contains one three- and one four-coordinate Cu(i) atom which are bridged by selenium atoms of two selenoacetato ligands similar to **2**. The Cu(i)–P and Cu(i)–Se distances are comparable to those observed in **2** and other related compounds.^{22–25} The effect of the substitution on the Se atom is not pronounced.

There appears to be a C–H···O hydrogen bond between one of the methyl hydrogen atoms and the oxygen atom of the CH₃C{O}Se[−] ligand. The hydrogen bonding parameters are: H(4b)···O(1) 2.54 Å, C(4)···O(1) 3.480(6) Å and C(4)–H(4b)···O(1) 168°. Such C–H···O interactions have been well documented by Steiner and Desiraju^{27,28} and help to influence

Table 2 Selected bond lengths (Å) and angles (°) for compound **6**

Bond lengths			
Cu(1)–P(1)	2.2983(7)	Se(2)–Cu(2)	2.4339(4)
Cu(1)–P(2)	2.2761(7)	Se(1)–C(1)	1.929(3)
Cu(2)–P(3)	2.2416(8)	Se(2)–C(3)	1.956(3)
Se(1)–Cu(1)	2.5482(4)	C(1)–O(1)	1.200(4)
Se(2)–Cu(1)	2.5358(4)	C(3)–O(2)	1.201(4)
Se(1)–Cu(2)	2.4278(4)	Cu(1)–Cu(2)	2.7043(4)
Bond Angles			
C(1)–Se(1)–Cu(2)	99.4(1)	P(1)–Cu(1)–Se(2)	105.52(2)
C(1)–Se(1)–Cu(1)	109.87(9)	P(2)–Cu(1)–Se(1)	118.51(2)
Cu(2)–Se(1)–Cu(1)	65.79(1)	P(1)–Cu(1)–Se(1)	97.52(2)
C(3)–Se(2)–Cu(2)	104.06(9)	Se(2)–Cu(1)–Se(1)	109.04(1)
C(3)–Se(2)–Cu(1)	108.24(9)	P(3)–Cu(2)–Se(1)	121.63(2)
Cu(2)–Se(2)–Cu(1)	65.90(1)	P(3)–Cu(2)–Se(2)	121.59(2)
P(2)–Cu(1)–P(1)	114.67(3)	Se(1)–Cu(2)–Se(2)	116.77(2)
P(2)–Cu(1)–Se(2)	110.30(2)		
Hydrogen Bond			
H(4b)···O(1)	2.54	C(4)···O(1)	3.480(6)
C(4)–H(4b)···O(1)	168		

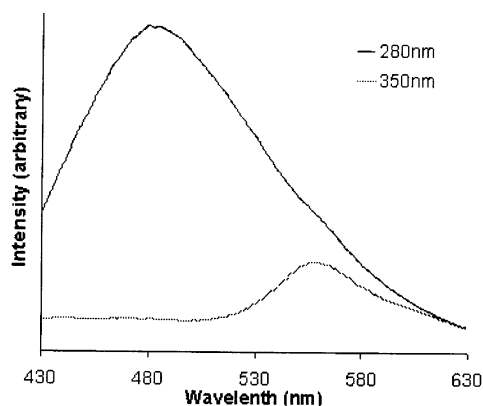


Fig. 5 Photoluminescence spectra of **1** in CH_2Cl_2 , excited at $\lambda = 280$ nm and 350 nm.

the packing in the solid state. The $\text{C}\cdots\text{O}$ distance observed in chloroalkyl compounds ranges from 3.32 to 3.59 Å, and the range of $\text{H}\cdots\text{O}$ is from 2.0 to 2.8 Å.²⁹ The hydrogen bonding parameters found in **6** fall in the normal range of $\text{C}\cdots\text{H}\cdots\text{O}$ bonding. This weak interaction seems to control the stereochemistry in the Cu_2Se_2 core. First, the two selenoacetato ligands have *syn* geometry instead of the *anti* configuration found in **2**. Secondly, the Cu_2Se_2 ring is no longer planar unlike **2** and has a butterfly conformation. Se(1) is 0.49 Å above the $\text{Cu}(1)\text{--Cu}(2)\text{--Se}(2)$ plane and Se(2) is 0.49 Å above the $\text{Cu}(1)\text{--Cu}(2)\text{--Se}(1)$ plane. In other words, the interplanar angle between the two Cu_2Se planes bisecting the $\text{Cu}(1)\cdots\text{Cu}(2)$ axis is 12.7° . The $\text{Cu}_2\text{Se}_2\text{P}_3$ core has an approximate *m* symmetry with the mirror plane passing through Cu(1) and Cu(2). As a consequence of the $\text{C}\cdots\text{H}\cdots\text{O}$ interaction, the $\text{Cu}(1)\cdots\text{Cu}(2)$ distance, 2.704 Å, is found to be longer than the value observed for compound **2**.

Photoluminescence studies

Photoluminescence spectra were measured at room temperature in CH_2Cl_2 solution. The concentration of the solution is 10^{-5} M, and the solid-state experiment was performed by evaporating the solution on a quartz plate. Two excitation wavelengths, 280 and 350 nm, were used for the experiments in solution.

A typical spectrum is shown in Fig. 5 for **1**. Table 3 lists the emission maxima observed for all the compounds in CH_2Cl_2 solution. For excitation at 280 nm, an emission signal at 481 nm is observed while at 350 nm an emission at 560 nm is observed for **1**. Similar shifts have been noted for other compounds too. As seen in Table 3, all the compounds have absorption peaks at 241–257 nm in the UV-Vis region and emission in the range 481–492 nm (for 280 nm excitation) and 560–564 nm (for 350 nm excitation). These may be attributed to MLCT transition.³⁰

Table 3 UV-Vis and photoluminescence spectra for compounds **1–5**

Medium (T/K)	$\lambda_{\text{abs}}/\text{nm}$ ($\epsilon \times 10^{-4}/$ $\text{ml mol}^{-1} \text{cm}^{-1}$)	$\lambda_{\text{em}}/\text{nm}$	
		Excited at 280 nm	Excited at 350 nm
1 CH_2Cl_2 (298)	245 (4.30)	481	560
2 CH_2Cl_2 (298)	241 (2.97), 259 (2.97)	486	560
3 CH_2Cl_2 (298)	241 (2.66), 264 (2.94)	487	564
4 CH_2Cl_2 (298)	257 (4.84)	492	560
5 CH_2Cl_2 (298)	244 (3.44)	483	561

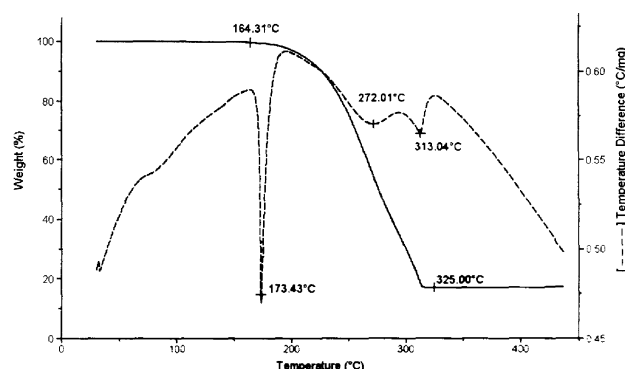


Fig. 6 TGA–DTA of **1**.

Thermal decomposition studies

Thermal analysis experiments were carried out in an N_2 atmosphere to prevent the oxidation of the sample. Typical TGA–DTA curves are shown in Fig. 6 and 7 respectively for **1** and **6**. The results have been compiled in Table 4.

All the compounds show only endotherms in DTA indicating that the decomposition of these compounds at any stage is an endothermic process. The first endotherms in the range 149–174°C are due to melting followed by decomposition. Both the DTA peak temperature and inception temperature of TG weight loss indicate that the alkyl derivative **6** is thermally less stable than the aromatic derivatives. Furthermore, there is no special trend found due to substituent effects at the *para* position.

Although the TG curves show only a single unresolved step of the weight loss in the temperature region 140–325°C, the corresponding DTA curves show two endotherms. This indicates the complexity of the thermal decomposition process. However it is clear that energy is needed to break the bonds in these complexes. The percentage of the residual weight at the end of the thermal decomposition process (inception of plateau after *ca.* 300–325°C) for each compound matches fairly well with the percentage weight of the residue calculated for the formation of $\text{Cu}_2\text{Se}/\text{Cu}_{2-x}\text{Se}$ (Table 4). The side products of decomposition possibly include Ph_3P , Ph_3PSe , and $(\text{RCO})_2\text{Se}$, based on the assumption that the selenocarboxylates decompose very similarly to thiocarboxylates as discussed by Hampden-Smith and coworkers.²

Pyrolysis experiment

Since the amounts used in thermal analysis experiment were in milligram quantities, sufficient amounts needed for further characterization of the final residues were obtained by the pyrolysis method. In this method, about 300 mg were heated at 300°C and 0.5 Torr pressure for 30 min and the final products

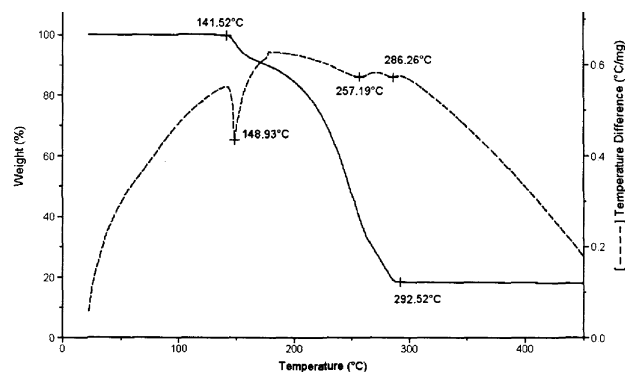


Fig. 7 TGA–DTA of **6**.

Table 4 TGA–DTA and pyrolysis results for compounds 1–6

Compounds	Thermogravimetry analysis		Pyrolysis experiment ^a						
	Temperature range/°C	DTA/°C ^b	Residual weight (%)		Weight of the residue (%)	Phase of residue	ICP result for the value of <i>x</i>	JCPDS No.	
			Observed	Calculated for Cu ₂ Se					
1	153–310	174(–), 273(–), 312(–)	17.1	16.1	17.0	Cubic Cu ₂ Se Cubic Cu _{2–<i>x</i>} Se	0.10	04-0839 06-0680	
2	154–300	183(–), 272(–), 306(–)	16.5	15.7	16.8	Cubic Cu ₂ Se Cubic Cu _{2–<i>x</i>} Se	0.24	04-0839 06-0680	
3	165–317	196(–), 280(–), 303(–)	18.3	15.4	16.0	Cubic Cu ₂ Se Cubic Cu _{2–<i>x</i>} Se	0.17	04-0839 06-0680	
4	159–325	183(–), 295(–), 395(–)	17.2	15.3	15.7	Cubic Cu ₂ Se Cubic Cu _{2–<i>x</i>} Se	0.10	04-0839 06-0680	
5	160–300	195(–), 269(–), 306(–)	17.0	15.6	16.1	Cubic Cu ₂ Se Cubic Cu _{2–<i>x</i>} Se	0.13	04-0839 06-0680	
6	141–287	149(–), 257(–), 286(–)	18.4	17.8	16.2	Cubic Cu ₂ Se Cubic Cu _{2–<i>x</i>} Se	0.16	04-0839 06-0680	

^a The samples were heated at 300 °C under 0.5 Torr pressure for 30 minutes. ^b (+) Exothermic, (–) endothermic.

were weighed. Again the weight of the residue in the pyrolysis method matched well with the expected residue weight calculated for the formation of copper selenides.

Characterization of the final products

X-Ray powder diffraction analysis was carried out on the residues obtained in the pyrolysis experiments. The results are shown in Table 4. The products are highly crystalline giving sharp intense signals. The XRD patterns (see ESI†) were compared with known copper selenide patterns from the database and the JCPDS numbers of matched phases are shown in Table 4. The entire residue has been found to be a mixture of the cubic phase of Cu₂Se (JCPDS No. 04-0839) and Cu_{2–*x*}Se (Berzelianite, JCPDS No. 06-0680) compounds. In the non-stoichiometric Cu_{2–*x*}Se compounds, the ratio of *x* was experimentally determined to be 0.1–0.24 by ICP experiments. The results are again tabulated in Table 4. There is no apparent difference in the nature of the final products due to substituents at the *para* position of the benzene rings.

SEM images (see ESI†) of the residues were obtained to find the nature of the final products as well as to investigate the influence of the substituents on the particle size. Particles with defined faces as big as 100 μm are seen in **1** and **2**. However the distribution of the particle sizes is not uniform. It varies from 1 μm to 100 μm in **1**, **2**, **3** and **6**. SEM images of the residues obtained from **4** and **5** show that they fall in a very narrow particle size distribution (1–20 μm) and the average particle size is ~5 μm. These samples were obtained from F and Cl substituted precursors. The exact effect of these substituents on the

particle size distribution of Cu₂Se and Cu_{2–*x*}Se is not clear at present. This interesting observation will certainly fuel further investigation.

Cu_{2–*x*}Se nanoparticles preparation

Trioctylphosphine (TOP)/trioctylphosphine oxide (TOPO) capped Cu_{2–*x*}Se nanoparticles were prepared by dissolving **1** in TOP and injecting into hot TOPO for thermal decomposition to obtain a dark green powder. XRPD and TEM were used to characterize the Cu_{2–*x*}Se nanoparticles. Fig. 8 shows the X-ray diffraction pattern of the product, which has been indexed as cubic Cu_{2–*x*}Se (06-0680). The TEM image is displayed in Fig. 9. The average particle size was found to be 75 ± 15 nm as calculated from the TEM images of more than 70 particles which showed particle sizes ranging from 40 to 100 nm (Fig. 10).

Summary

In this report the synthesis of a number of neutral dimers, [(Ph₃P)₂Cu(μ-SeC(O)R)₂Cu(PPh₃)], has been described. The chemistry of the Ph₃P:Cu(I):RC(O)Se[–] system is found to be different from that of the corresponding sulfur analogue. In the corresponding thiocarboxylate system, a number of compounds with varying nuclearity and bonding modes have been observed. However, the unsymmetrical neutral dimer is the

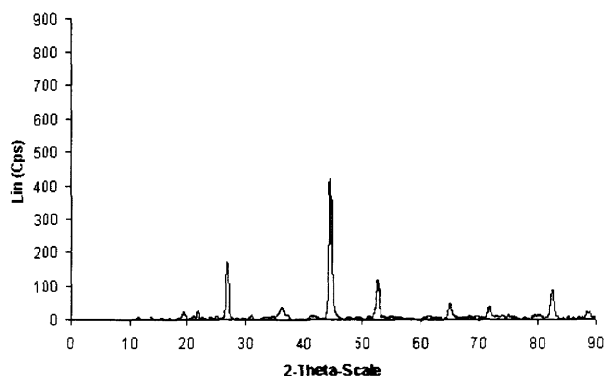


Fig. 8 XRPD for TOP/TOPO capped Cu_{2–*x*}Se nanoparticles.

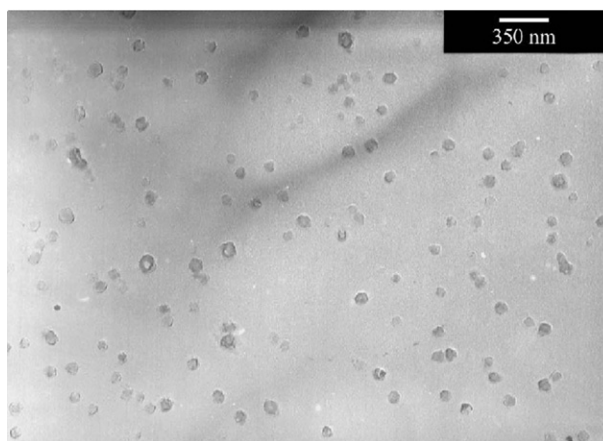


Fig. 9 TEM for TOP/TOPO capped Cu_{2–*x*}Se nanoparticles.

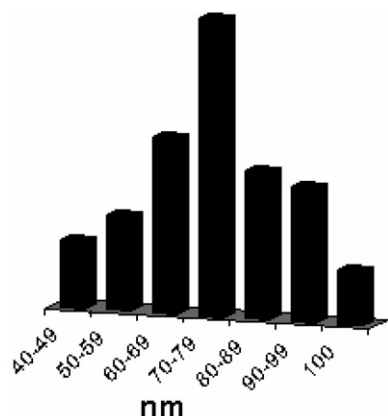


Fig. 10 Histogram of particle sizes of Cu_{2-x}Se nanoparticles from 1.

only product obtained by changing the $\text{Ph}_3\text{P}:\text{Cu}(\text{SeC}\{\text{O}\}\text{R})$ ratios during the preparation. Variable temperature ^{31}P NMR indicates that the phosphine ligands undergo fast exchange in solution above 270 K. It appears that the unsymmetrical dimer dissociates in solution but the Cu_2Se_2 core is intact. Weak $\text{C}-\text{H}\cdots\text{O}$ hydrogen bonding is found to dictate the stereochemistry of the RCO groups in the Cu_2Se_2 rings. These compounds are photoemissive in the region 480–492 nm when excited at 280 nm and ~ 560 nm when excited at 350 nm in CH_2Cl_2 solution. Pyrolysis and TG experiments suggest that these neutral dimers can be good single source molecular precursors to $\text{Cu}_2\text{Se}/\text{Cu}_{2-x}\text{Se}$ bulk materials. Preliminary experiments show that $[(\text{Ph}_3\text{P})_2\text{Cu}(\mu\text{-SeC}\{\text{O}\}\text{Ph})_2\text{Cu}(\text{PPh}_3)]$ can produce nanoparticles.

Experimental

Sodium, selenium (gray), naphthalene powder, acyl chloride, copper nitrate, triphenylphosphine, trioctylphosphine oxide (TOPO, 90%), trioctylphosphine (TOP) were obtained commercially and used as received. THF was dried by refluxing with sodium metal using benzophenone as indicator and distilling before use and the other solvents were dried by allowing them to stand over 3 Å molecular sieves overnight.

Synthesis

The synthetic procedure described in detail for 1 was also used to prepare compounds 2 to 6.

[$\text{Cu}_2(\mu\text{-SeC}\{\text{O}\}\text{Ph})_2(\text{PPh}_3)_3$] 1. Sodium selenocarbonylate was prepared *in situ* by the literature method as follows.³¹ In a N_2 flushed 2-necked flask Na_2Se (0.150 g, 1.2 mmol) and benzoyl chloride (0.093 mL, 0.8 mmol) were mixed in MeCN (15 mL) at 0°C and stirred for an hour. Then the mixture was filtered and to the filtrate a solution of $(\text{Ph}_3\text{P})_2\text{CuNO}_3$ (0.455 g, 0.7 mmol) in MeCN (10 mL) was added, and stirred for 30 min. The orange precipitate formed was filtered, washed with MeCN, H_2O and Et_2O , and recrystallized from a mixture of CH_2Cl_2 and Et_2O . Yield: 0.43 g (48%). Anal. Calcd. for $\text{C}_{68}\text{H}_{55}\text{Cu}_2\text{O}_2\text{P}_3\text{Se}_2$ (mol wt 1282.12): C, 63.70; H, 4.32. Found: C, 63.74; H, 3.96%. ^1H NMR (CD_2Cl_2): δ /ppm. For selenobenzoato ligand: 7.67 (4H, *o*); 7.09–7.29 (51H, PPh_3 (45H), 4H, *o*, 2H, *p*). ^{13}C NMR (CDCl_3): δ /ppm. For selenobenzoato ligand: 127.12 ($\text{C}_{2/6}$ or $\text{C}_{3/5}$), 128.61 ($\text{C}_{2/6}$ or $\text{C}_{3/5}$), 131.05 (C_4), 142.94 (C_1), 201.50 (COSe). For PPh_3 : 128.15 (C_3 , $^3J(\text{P}-\text{C}) = 8.7$ Hz), 129.30 (C_4), 133.14 (C_1 , $^1J(\text{P}-\text{C}) = 28.4$ Hz), 133.95 (C_2 , $^2J(\text{P}-\text{C}) = 14.2$ Hz). ^{31}P NMR (CD_2Cl_2): δ /ppm. -0.63 . IR data: cm^{-1} . 3051, 1625(C=O), 1608, 1592, 1572, 1479, 1443, 1434, 1305, 1189, 1164, 1094,

1070, 1026, 998, 927, 878, 768, 742, 689, 670, 624, 517, 487, 435, 419. UV-Vis $\lambda_{\text{max}}(\log \epsilon) = 244$ (4.63) nm.

[$\text{Cu}_2(\mu\text{-SeC}\{\text{O}\}\text{C}_6\text{H}_4\text{-CH}_3\text{-4})_2(\text{PPh}_3)_3$] 2. Dark brown crystals. Yield: 56%. Anal. Calcd. for $\text{C}_{70}\text{H}_{59}\text{Cu}_2\text{O}_2\text{P}_3\text{Se}_2$ (mol wt 1310.17): C, 64.17; H, 4.54. Found: C, 63.87; H, 5.21%. ^1H NMR (CD_2Cl_2): δ /ppm. for *p*-methylselenobenzoato ligand: 2.23 (6H, CH_3), 6.93 (4H, *m*), 7.60 (4H, *o*); for PPh_3 : 7.08–7.31 (45H). ^{13}C NMR (CDCl_3): δ /ppm. For *p*-methylselenobenzoato ligand: 21.37 (CH_3), 127.80 ($\text{C}_{2/6}$ or $\text{C}_{3/5}$), 128.72 ($\text{C}_{2/6}$ or $\text{C}_{3/5}$), 140.71 (C_1), 141.32 (C_4), 201.97 (COSe). For PPh_3 : 128.19 (C_3 , $^3J(\text{P}-\text{C}) = 8.7$ Hz), 129.24 (C_4), 133.29 (C_1 , $^1J(\text{P}-\text{C}) = 28.4$ Hz), 133.91 (C_2 , $^2J(\text{P}-\text{C}) = 15.3$ Hz). ^{31}P NMR (CDCl_3): δ /ppm. -0.69 . IR data: cm^{-1} . 3051, 1623(C=O), 1609, 1597, 1568, 1479, 1457, 1434, 1404, 1303, 1288, 1212, 1194, 1162, 1094, 1070, 1027, 997, 882, 825, 784, 742, 694, 612, 564, 541, 514, 504, 493, 467, 418. UV-Vis $\lambda_{\text{max}}(\log \epsilon) = 260$ (4.47), 242 (4.48) nm.

[$\text{Cu}_2(\mu\text{-SeC}\{\text{O}\}\text{C}_6\text{H}_4\text{-OCH}_3\text{-4})_2(\text{PPh}_3)_3$] 3. Greenish yellow crystals. Yield: 58%. Anal. Calcd. for $\text{C}_{70}\text{H}_{59}\text{Cu}_2\text{P}_3\text{Se}_2$ (mol wt 1342.17): C, 62.64; H, 4.43. Found: C, 62.76; H, 4.50%. ^1H NMR δ /ppm. (CD_2Cl_2): For *p*-methoxyselenobenzoato ligand: 3.77 (6H, OCH_3), 6.63 (4H, *m*), 7.72 (4H, *o*); for PPh_3 : 7.12–7.39 (45H). ^{13}C NMR (CDCl_3): δ /ppm. For *p*-methoxyselenobenzoato ligand: 55.20 (OCH_3), 112.26 ($\text{C}_{3/5}$), 130.94 ($\text{C}_{2/6}$), 132.06 (C_1), 162.26 (C_4). For PPh_3 : 128.28 (C_3 , $^3J(\text{P}-\text{C}) = 8.7$ Hz), 129.36 (C_4), 133.03 (C_1 , $^1J(\text{P}-\text{C}) = 28.4$ Hz), 133.85 (C_2 , $^2J(\text{P}-\text{C}) = 15.3$ Hz). ^{31}P NMR (CD_2Cl_2): δ /ppm. -1.29 . IR data: cm^{-1} . 3051, 3000, 2834, 1617(C=O), 1610, 1592, 1569, 1500, 1479, 1459, 1434, 1412, 1307, 1261, 1246, 1199, 1180, 1155, 1109, 1093, 1070, 1036, 1024, 997, 971, 882, 840, 810, 788, 782, 743, 694, 645, 624, 611, 513, 503, 487, 450, 418. UV-Vis $\lambda_{\text{max}}(\log \epsilon) = 266$ (4.47), 241 (4.43) nm.

[$\text{Cu}_2(\mu\text{-SeC}\{\text{O}\}\text{C}_6\text{H}_4\text{-Ph-Cl-4})_2(\text{PPh}_3)_3$] 4. Brown crystals. Yield: 44%. Anal. Calcd. for $\text{C}_{68}\text{H}_{53}\text{Cu}_2\text{O}_2\text{P}_3\text{Se}_2\text{Cl}_2$ (mol wt 1351.01): C, 60.45; H, 3.95; Cl: 5.25. Found: C, 59.94; H, 3.91; Cl: 5.25%. ^1H NMR (CD_2Cl_2): δ /ppm. For *p*-chloroselenobenzoato ligand: 7.07 (4H, *m*), 7.59 (4H, *o*); for PPh_3 : 7.12–7.37 (45H). ^{13}C NMR (CDCl_3): δ /ppm. For *p*-chloroselenobenzoato ligand: 127.15 ($\text{C}_{3/5}$), 129.88 ($\text{C}_{2/6}$), 137.19 (C_1), 141.25 (C_4), 200.37 (COSe). For PPh_3 : 128.18 (C_3 , $^3J(\text{P}-\text{C}) = 9.8$ Hz), 129.32 (C_4), 133.11 (C_1 , $^1J(\text{P}-\text{C}) = 29.4$ Hz), 133.87 (C_2 , $^2J(\text{P}-\text{C}) = 14.2$ Hz). ^{31}P NMR (CD_2Cl_2): δ /ppm. -0.63 . IR data: cm^{-1} . 3052, 3003, 1629(C=O), 1600, 1582, 1567, 1479, 1434, 1393, 1326, 1306, 1277, 1187, 1158, 1093, 1027, 1012, 998, 973, 877, 838, 743, 723, 693, 628, 617, 551, 517, 487, 424. UV-Vis $\lambda_{\text{max}}(\log \epsilon) = 258$ (4.69) nm.

[$\text{Cu}_2(\mu\text{-SeC}\{\text{O}\}\text{C}_6\text{H}_4\text{-F-4})_2(\text{PPh}_3)_3$] 5. Bright yellow crystals. Yield: 63%. Anal. Calcd. for $\text{C}_{68}\text{H}_{53}\text{Cu}_2\text{O}_2\text{P}_3\text{Se}_2\text{F}_2$ (mol wt 1318.10): C, 61.96; H, 4.05; F: 2.88. Found: C, 61.84; H, 3.68; F: 2.80%. ^1H NMR (CD_2Cl_2) δ /ppm. For *p*-fluoroselenobenzoato ligand: 6.79 (4H, *m*), 7.69 (4H, *o*); for PPh_3 : 7.12–7.38 (45H). ^{13}C NMR (CDCl_3): δ /ppm. for *p*-fluoroselenobenzoato ligand: 113.78 ($\text{C}_{3/5}$, $J = 21.8$ Hz), 130.92 ($\text{C}_{2/6}$, $J = 8.7$ Hz), 139.34 (C_1), 164.74 (C_4 , $J = 251.9$ Hz), 200.08 (COSe). For PPh_3 : 128.18 (C_3 , $^3J(\text{P}-\text{C}) = 9.8$ Hz), 129.30 (C_4), 133.19 (C_1 , $^1J(\text{P}-\text{C}) = 28.4$ Hz), 133.89 (C_2 , $^2J(\text{P}-\text{C}) = 14.0$ Hz). ^{31}P NMR (CD_2Cl_2): δ /ppm. -0.73 . IR data: cm^{-1} . 3053, 2923, 1624(C=O), 1612, 1587, 1496, 1480, 1434, 1403, 1312, 1288, 1221, 1183, 1148, 1095, 1028, 998, 886, 843, 803, 745, 694, 637, 610, 518, 493, 463, 434. UV-Vis $\lambda_{\text{max}}(\log \epsilon) = 244$ (4.54) nm.

[$\text{Cu}_2(\mu\text{-SeC}\{\text{O}\}\text{CH}_3)_2(\text{PPh}_3)_3$] 6. Grey crystals. Yield: 30%. Anal. Calcd. for $\text{C}_{58}\text{H}_{51}\text{Cu}_2\text{O}_2\text{P}_3\text{Se}_2$ (mol wt 1157.98): C, 60.16; H, 4.44. Found: C, 59.43; H, 3.97%. ^1H NMR (CD_2Cl_2):

δ /ppm 1.94 (6H, CH₃), 7.21–7.40 (45H, (C₆H₅)₃P). ¹³C NMR (CDCl₃): δ /ppm 40.42 (CH₃, *J* = 14.2 Hz), 204.40 (COSe). For PPh₃: 128.26 (C₃, ³*J*(P–C) = 9.8 Hz), 129.39 (C₄), 133.30 (C₁, ¹*J*(P–C) = 27.3 Hz), 133.92 (C₂, ²*J*(P–C) = 15.3 Hz). ³¹P NMR (CD₂Cl₂): δ /ppm. –1.51. IR data: cm^{–1}. 3050, 2923, 2854, 1682(C=O), 1657, 1586, 1572, 1480, 1434, 1338, 1311, 1183, 1158, 1094, 1028, 998, 931, 850, 743, 694, 584, 565, 516, 431, 422.

Nanoparticle preparation

A typical preparation of TOP/TOPO capped metal selenides has been reported in the literature³² and the procedure is described as follows. The reaction vessel containing 1 g of TOPO was heated and stabilized at 220–230 °C and ambient pressure under nitrogen. **1** (0.3 g) was dissolved in TOP (5 mL) using an ultrasonic bath, then loaded into a 10 mL syringe, then quickly injected into the vigorously stirring hot TOPO through a rubber septum. The stirring was continued for an hour at 220–230 °C and then the mixture was allowed to cool down to 60–70 °C. Methanol was added into the mixture, and a flocculate was formed which was separated by centrifugation. This residue was washed with MeOH 2–3 times and dried in a vacuum desiccator. The sample for TEM was prepared by placing a drop of a dilute toluene dispersion of nanocrystallites on the surface of a grid, waiting for ~1 min, and then wicking away the solution.

Physico-chemical measurements

The ¹³C{¹H}, ¹H and ³¹P{¹H} NMR spectra were recorded on a Bruker ACF300 FT-NMR instrument using TMS as internal reference at 25 °C in CD₂Cl₂ or CDCl₃. The IR spectra (KBr pellet) were recorded using a Bio-Rad FT-IR spectrophotometer. UV-Vis spectra were recorded using a Shimadzu UV-2501PC model spectrophotometer in CH₂Cl₂ solution. The elemental analyses were performed in the microanalytical lab in the Department of Chemistry, National University of Singapore. Photoluminescence spectra were recorded on a Perkin Elmer Luminescence Spectrometer LS50B–50 Hz.

Thermogravimetry analysis was recorded on a SDT 2960 Simultaneous DTA–TGA with a heating rate of 10 °C min^{–1} under N₂ atmosphere. The pyrolysis experiment was carried out in a self-designed apparatus with a heating rate of 10 °C min^{–1} under a mild vacuum of about 0.5 Torr. XRPD was recorded on a D5005 Bruker AXS X-ray diffractometer, with a scanning angle range from 2 to 90°. SEM images were recorded on a JEOL JSM-T220A Scanning Microscope, with an accelerating voltage of 20 kV. The TEM image was taken on a Jeol STEM CXII Electro Microscope using an accelerating voltage of 100 kV. Copper grids (200 mesh) coated with amorphous carbon film were purchased from Solid Vision.

X-Ray crystallography

The single crystal X-ray diffraction experiments were carried out on a Bruker SMART CCD diffractometer with Mo K_α radiation, in a sealed tube at 20 °C. The software SMART³³ was used for collecting frames of data, indexing reflections, and determining the lattice parameters, SAINT³⁵ for integration of the intensity of reflections and scaling, SADABS³⁴ for absorption correction, and SHELXTL³⁵ for space group and structure determination and least-squares refinements on *F*². All the hydrogen atoms were fixed at the calculated positions for the purpose of structure factor calculations only. In the final difference Fourier map the electron densities fluctuate in the range 0.336 to –0.318 for **2** and 0.380 to –0.265 for **6**. Crystal data and refinement details are displayed in Table 5.

Table 5 Crystal data and refinement details

	2	6
Chemical formula	C ₇₀ H ₅₉ Cu ₂ O ₂ P ₃ Se ₂	C ₅₈ H ₅₁ Cu ₂ O ₂ P ₃ Se ₂
Formula weight	1310.08	1157.90
<i>T</i> /K	293(2)	293(2)
Crystal system	Triclinic	Monoclinic
Space group	<i>P</i> $\bar{1}$	<i>P</i> ₂ / <i>c</i>
<i>a</i> /Å	10.8966(1)	19.4676(2)
<i>b</i> /Å	12.9988(2)	14.5399(1)
<i>c</i> /Å	22.3564(3)	20.0449(2)
α /°	90.883(1)	
β /°	101.145(1)	111.690(1)
γ /°	99.031(1)	
<i>V</i> /Å ³	3064.97(7)	5272.12(8)
<i>Z</i>	2	4
<i>D</i> _c /g cm ^{–3}	1.420	1.459
μ /mm ^{–1}	2.004	2.320
Reflections measured	15 098	26 569
Independent reflections	10 055 (<i>R</i> _{int} = 0.0272)	9260 (<i>R</i> _{int} = 0.0260)
Data/restraints/parameters	10 055/0/713	9260/0/607
GooF	1.121	0.988
Final <i>R</i> indices	<i>R</i> ₁ = 0.0560, <i>wR</i> ₂ = 0.0872	<i>R</i> ₁ = 0.0288, <i>wR</i> ₂ = 0.0695
<i>R</i> indices (all data)	<i>R</i> ₁ = 0.0890, <i>wR</i> ₂ = 0.0988	<i>R</i> ₁ = 0.0416, <i>wR</i> ₂ = 0.0769

CCDC reference numbers 171911 and 171912. See <http://www.rsc.org/suppdata/nj/b2/b2034666/> for crystallographic data in CIF or other electronic format.

Acknowledgements

J. J. V. would like to thank NUS for financial support through the grant R143-000-084-112. Dr. T. C. Deivaraj of this department and Prof. Phil Dean from the University of Western Ontario, London, Canada are thanked for their interest in this project.

References

- M. D. Nyman, M. J. Hampden-Smith and E. N. Duesler, *Chem. Vap. Deposit.*, 1996, **2**(5), 171.
- M. D. Nyman, M. J. Hampden-Smith and E. N. Duesler, *Inorg. Chem.*, 1997, **36**, 2218.
- T. C. Deivaraj, G. X. Lai and J. J. Vittal, *Inorg. Chem.*, 2000, **39**, 1028.
- G. Speier, V. Fülöp and G. Argay, *Transition Met. Chem.*, 1991, **16**, 576.
- J. T. Sampanthar, J. J. Vittal and P. A. W. Dean, *J. Chem. Soc., Dalton Trans.*, 1999, 3153.
- J. J. Vittal and P. A. W. Dean, *Inorg. Chem.*, 1996, **35**, 3089.
- I. Jibril, F. T. Esmadi, H. Al-Masri, L. Zsolnai and G. Huttner, *J. Organomet. Chem.*, 1996, **510**, 109.
- F. T. Esmadi and M. L. Sumadi, *Synth. React. Inorg. Met-Org. Chem.*, 1994, **24**, 715.
- Y. Kawahara, S. Kato, T. Kanda, T. Murai and K. Miki, *J. Chem. Soc., Dalton Trans.*, 1996, **79**.
- W. Eikens, S. Jäger, P. G. Jones and C. Thöne, *J. Organomet. Chem.*, 1996, **511**, 67.
- S. T. Lakshmi Kumar, *Sol. Energy Mater. Sol. Cells*, 1994, **32**, 7.
- T. Hayashi and H. Yao, *Jpn. Kokai Tokkyo Koho*, JP 02 173 622; 1990, CA No. 114:72112.
- A. A. Korzhuev, *Fiz. Khim. Obrab. Mater.*, 1991, **3**, 131.
- Z. Qiao, Y. Xie, J. Xu, X. Liu, Y. Zhu and Y. Qian, *Can. J. Chem.*, 2000, **78**, 1143.
- V. Dusastre, B. Omar, I. P. Parkin and G. A. Shaw, *J. Chem. Soc., Dalton Trans.*, 1997, 3503.

- 16 Y. Cheng, T. J. Emge and J. G. Brennan, *Inorg. Chem.*, 1996, **35**, 7339.
- 17 M. A. Malik, P. O'Brein and N. Revaprasadu, *Adv. Mater.*, 1999, **11**(17), 1441.
- 18 T. C. Deivaraj and J. J. Vittal, unpublished results.
- 19 (a) S. Kato, H. Ishihara, K. Ibi, H. Kageyama and T. Murai, *J. Organomet. Chem.*, 1990, **332**, 898; (b) S. Kato, T. Murai and M. Ishida, *Org. Prep. Proced. Int.*, 1986, **18**, 369.
- 20 H. Ishihara and Y. Hirabayashi, *Chem. Lett.*, 1976, **203**.
- 21 Y. Kawahara, S. Kato, T. Kanda and T. Murai, *Bull. Chem. Soc. Jpn.*, 1994, **67**, 1881.
- 22 J. Kampf, R. Kumar and J. P. Oliver, *Inorg. Chem.*, 1992, **31**, 3626.
- 23 W. Hirpo, S. Dhingra, A. C. Sutorik and M. G. Kanatzidis, *J. Am. Chem. Soc.*, 1993, **115**, 1597.
- 24 J. Cusick, M. L. Scudder, D. C. Craig and I. G. Dance, *Polyhedron*, 1989, **8**, 1139.
- 25 U. Müller, M.-L. Ha-Eierdanz, G. Kräuter and K. Dehnicke, *Z. Naturforsch. B*, 1990, **45**, 1128.
- 26 A. Bondi, *J. Phys. Chem.*, 1964, **68**, 441.
- 27 T. Steiner, *Chem. Commun.*, 1997, 727.
- 28 G. R. Desiraju, *Angew. Chem., Int. Ed. Engl.*, 1995, **34**, 2311.
- 29 G. R. Desiraju and T. Steiner, in *The Weak Hydrogen Bond in Structural Chemistry and Biology*, Oxford Science Publications, 1999, p. 25.
- 30 R. A. Rader, D. R. McMillin, M. T. Buckner, T. G. Matthews, D. J. Casadonte, R. K. Lengel, S. B. Whittaker, L. M. Darmon and F. B. Lytle, *J. Am. Chem. Soc.*, 1981, **103**, 5906.
- 31 O. Niyomura, K. Tani and S. Kato, *Heteroatom Chem.*, 1999, **10**(5), 373.
- 32 C. B. Murray, D. J. Norris and M. G. Bawendi, *J. Am. Chem. Soc.*, 1993, **115**, 8706.
- 33 *SMART & SAINT Software Reference Manual*, Version 6.22, Bruker Analytical X-ray Systems, Inc., Madison, WI, 2001.
- 34 G. M. Sheldrick, SADABS software for empirical absorption correction, University of Göttingen, Göttingen, Germany, 2000.
- 35 *SHELXTL Software Reference Manual*, Version 5.1, Bruker Analytical X-ray Systems, Ind., Madison, WI, 1997.